Applied Physics Letters

Jet-driven viscous locomotion of confined thermoresponsive microgels

Cite as: Appl. Phys. Lett. **120**, 104101 (2022); https://doi.org/10.1063/5.0076244
Submitted: 22 October 2021 • Accepted: 28 January 2022 • Published Online: 08 March 2022
Published open access through an agreement with University of Cambridge

Ivan Tanasijević, Oliver Jung, Lyndon Koens, et al.

Applied Physics Letters ARTICLE scitation.org/journal/apl

Jet-driven viscous locomotion of confined thermoresponsive microgels

Cite as: Appl. Phys. Lett. **120**, 104101 (2022); doi: 10.1063/5.0076244
Submitted: 22 October 2021 · Accepted: 28 January 2022 ·
Published Online: 8 March 2022

View Online Export Citation CrossMark

Ivan Tanasijević,[1] Oliver Jung,[2] Lyndon Koens,[3,4] Ahmed Mourran,[2] and Eric Lauga[1,a)]

AFFILIATIONS

[1]Department of Applied Mathematics and Theoretical Physics, University of Cambridge, Wilberforce Road, Cambridge CB3 0WA, United Kingdom
[2]DWI Leibniz-Institute for Interactive Materials, RWTH Aachen University, Forckenbeckstr. 50, D-52056 Aachen, Germany
[3]Macquarie University, Macquarie Park, NSW 2113 Sydney, Australia
[4]Department of Physics and Mathematics, University of Hull, Hull HU6 7RX, United Kingdom

[a)]Author to whom correspondence should be addressed: e.lauga@damtp.cam.ac.uk

ABSTRACT

We consider the dynamics of micro-sized, asymmetrically coated thermoresponsive hydrogel ribbons (microgels) under periodic heating and cooling in the confined space between two planar surfaces. As the result of the temperature changes, the volume and, thus, the shape of the slender microgel change, which leads to repeated cycles of bending and elastic relaxation, and to net locomotion. Small devices designed for biomimetic locomotion need to exploit flows that are not symmetric in time (non-reciprocal) to escape the constraints of the scallop theorem and undergo net motion. Unlike other biological slender swimmers, the non-reciprocal bending of the gel centerline is not sufficient here to explain for the overall swimming motion. We show instead that the swimming of the gel results from the flux of water periodically emanating from (or entering) the gel itself due to its shrinking (or swelling). The associated flows induce viscous stresses that lead to a net propulsive force on the gel. We derive a theoretical model for this hypothesis of jet-driven propulsion, which leads to excellent agreement with our experiments.

Self-propulsion allows micro-organisms to explore their environments, from small bacteria[1] to larger aquatic organisms.[2] Since early quantitative studies in the 1950s,[3,4] theoretical and experimental studies of various micro-organisms have led to discoveries of the numerous physical mechanisms used by motile cells to self-propel through viscous fluids,[5,6] in particular algae,[7,8] bacteria,[9] and spermatozoa.[10] The quantitative investigation of such phenomena has led to a better understanding of biological and physiological phenomena, including human reproduction[11] and infectious diseases.[12] Beyond biology, the field of biomimetic design is showing a lot of promises in mimicking these mechanisms to create controllable artificial microswimmers,[13–17] which are now starting to find use in medical applications[18] such as targeted drug delivery[19] and minimally invasive surgeries.[20]

One of the major practical design limitations for small-scale biomimetic propulsion was formulated by Purcell.[21] It states that if an artificial swimmer undergoes periodic shape changes that are "reciprocal" over a single period (i.e., that remain identical under a time-reversible symmetry), the overall displacement of the swimmer is necessarily zero. The justification of this theorem lies in the time-reversibility of the Stokes equations that describe the motion of the surrounding fluid at the micro-scale. As a result, one of the games to play for biomimetic propulsion is to circumvent the limitations of the scallop theorem.[22] The most obvious way is to use a propulsive mechanism that leads to non-reciprocal kinematics,[23–31] which, in many cases, is facilitated by the elastic compliance of the swimmer.[32–35] Other common ways include exploiting inertia[36,37] or the non-Newtonian properties of the surrounding fluid.[38,39]

In this paper, we investigate the motion of artificial microswimmers based on a thermoresponsive hydrogel actuated under reciprocal cycles of heating and cooling. We first explore experimentally the propulsive features of these swimmers and find that the external actuation results in a slightly non-reciprocal shape change. Using standard modeling of the hydrodynamic forces and flows for slender objects, we next show that the non-reciprocity in shape change is not sufficient to account for the overall swimming motion. Instead, we demonstrate that the propulsion originates from the local flows induced by the swelling and deswelling of the gel, with a mathematical model that leads to excellent agreement with experiments.

Microswimmers were produced as slender ribbons made of crosslinked poly(N-isopropyacrylamide) PNIPAm,[40–44] laden with

gold nanorods and sputtered with a layer of gold on one of its largest sides, as illustrated in Fig. 1(a). The microswimmers were placed in the tight space between two flat rigid surfaces [Fig. 1(b)], so that the resulting motion can be considered to be quasi-two-dimensional (2D). For more information on the experimental methods, we refer the reader to the supplementary material.

In order to actuate the microswimmers, we take advantage of the thermoresponsivity of the hydrogel. An increase in temperature reduces the solubility of the polymer, thereby shifting the equilibrium state, i.e., the balance between the free energy of mixing the solvent molecules and polymer chains and the elastic free energy of the network.[45–48] Due to the entropic nature of the hydrophobic interaction, water is transported out of the gel upon collapse, until a new balance between elastic and osmotic forces has been reached. In the case of a temperature-driven volume phase transition, the temperature change depends on heat transfer, which is orders of magnitude faster than mass transport. Consequently, the imbalance between osmotic and elastic forces depends considerably on the rate of the temperature change and the dimensions of the microgel.

The key property that allows for the directional motion of the microgels is the anisometry of their bodies, which we control by using particle replication in non-wetting template.[49] Such technique is valuable for the synthesis of a well-defined composition and shape. It allows the integration of plasmonic nanoparticles for optical heating and the possibility of a second passive layer. Such a bilayer bends with the temperature [see Fig. 1(c)], converting volume change into elastic energy.[42] Under near infrared laser (NIR) irradiation, the gold nanorods absorb light energy and heat the polymer matrix, while the surrounding fluid acts as a heat sink.[44,50] Rapid optical heating inevitably creates heterogeneities because the response of the polymer is slow, requiring diffusion of water molecules out of the network.[51] The anisometry of the microgels and the transient heterogeneity cause stress accumulation resulting in body deformation. The process, although with hysteresis, is reversible, and the shape recovers as soon as the irradiation ends.[41]

In our experiments, we induce a periodic shape deformation of the microgel, of period $T = t_{on} + t_{off}$, by irradiating it steadily with a NIR light for a time t_{on} and letting it recover for a time t_{off}. An example of the resulting shape deformation is shown in Fig. 1(d), where we extracted the centerline of the microgel from experimental videos and averaged over a large number of periods (>100). For a range of irradiation and recovery times, we discover a non-vanishing net

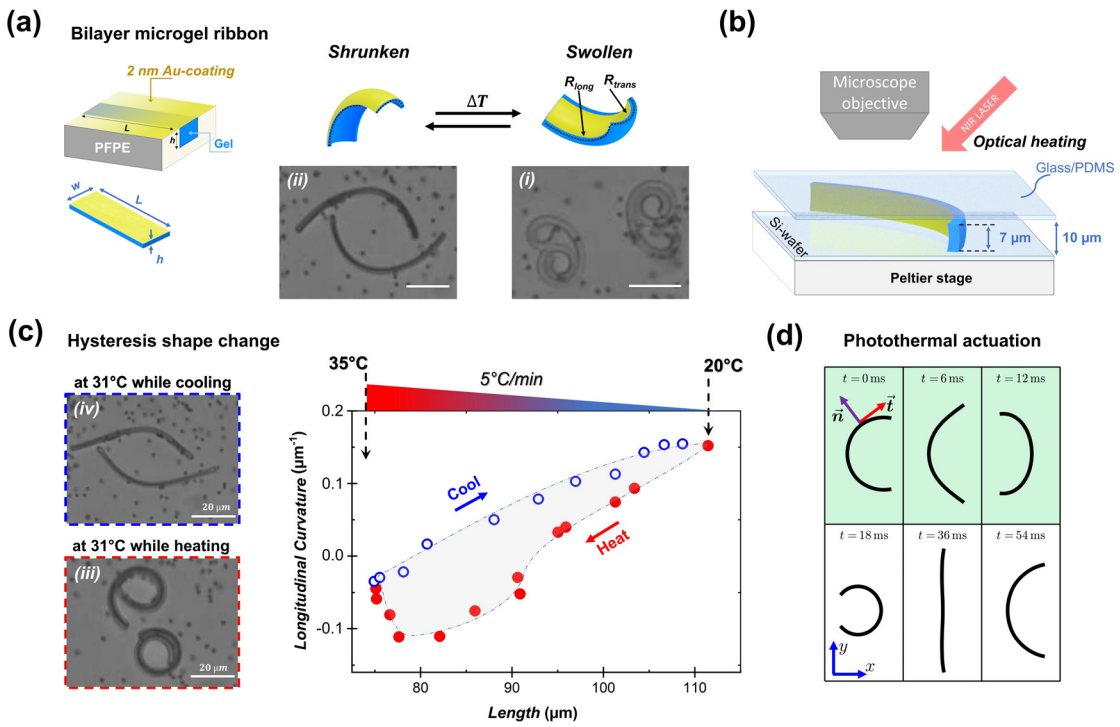

FIG. 1. (a) A microgel ribbon made of crosslinked PNIPAm synthesized in a fluoroelastomer mold and sputtered with a 2 nm thick gold as a passive layer. The ribbon has a length $L = 80\ \mu$m, a width $w = 5\ \mu$m, and a thickness $t = 2\ \mu$m. When released into cold water, the gel swells and bends (with the gold layer inward) along the longitudinal and transverse axes with a curvature R_{long} and R_{trans}, respectively. Above 32 °C, the microgel shrinks and the curvatures reverse, with the gold layer outward. (b) Experimental setup including a controlled heating stage, a microscope for optical observation and NIR laser irradiation at 45°. The microgels are loaded into the microcompartment in which the ribbons spontaneously orient themselves edge-on relative to the confining surfaces, creating a gap of about 1.5 μm above and below the swollen gel. (c) Variation of the longitudinal curvature (with $C_{long} = 1/R_{long}$) as a function of the ribbon length L during a 5 °C/min heating (full, red symbols)/cooling (empty, blue symbols) ramp from 20 to 35 °C. Optical micrographs show the characteristic shapes of the ribbons swollen at 20 °C (i) and shrunken at 35 °C (ii). The graph shows the hysteresis of the ribbon curvature, along with the optical micrographs (iii) and (iv), taken at 31 °C, where the ribbon length is close to the preparation state ($L = 80\ \mu$m) but shows a significant difference in curvature depending on whether it is being cooled or heated. (d) Shape of the gel centerline during periodic photothermal actuation, extracted from the experimental videos and averaged over many periods, for $t_{off} = 60$ ms and $t_{on} = 12$ ms. Light green background indicates the part of the period when the microgel is heated (laser is on).

displacement of the gel over a single period of actuation. We illustrate these results in Fig. 2 for $t_{off} = 60$ and $t_{on} = 10$ ms. In Fig. 2(a), we show a time lapse of the gel's motion, while we plot the average instantaneous speed U of the gel in Fig. 2(b) and the average displacement of its geometric center-of-mass in Fig. 2(c).

It is clear from Fig. 2(a) that the gel translates in a direction that is not parallel to its apparent axis of symmetry. Given our setup, this might appear unexpected as the system is quasi-2D, and the 2D shape of the gel appears to remain symmetric with respect to its initial axis of symmetry [i.e., the x axis in Fig. 1(d)]. However, in our previous studies,[43,44] we observed that even the equilibrium shapes of such microgels are slightly chiral. We believe that the microgels investigated in this paper are also slightly chiral, around the axis perpendicular to the plane of observation, which causes the observed misalignment between the apparent axis of symmetry and the direction of translation. For a different choice of t_{on}, we observe a motion that is a combination of rotation and translation (see Fig. S1(a) in the supplementary material). Similarly, we believe that the chirality is responsible for this as well.

Since the gel undergoes a non-reciprocal shape change [as illustrated in Fig. 1(c)], we might suspect that these shape changes, combined with the drag from the surrounding fluid, are sufficient to explain the observed net translation. We tested this using resistive-force theory of slender filaments[52] to compute the viscous drag on the gel as a function of its shape and of the ratio of drag coefficients $\Gamma = \xi_\perp/\xi_\parallel > 1$. In an infinite fluid $\Gamma \approx 2$, but, due to the immediate presence of the walls, this drag coefficient ratio could be different from this bulk value and could also be time-dependent since the microgel changes shape throughout a period of actuation. However, independently of our choice for Γ, we find that the predicted velocities so obtained are one order of magnitude smaller than what we see in the experiments. We, therefore, conclude that the net motion of the gel is induced by different physical mechanisms.

We propose here that the swimming of the gel results instead from the flux of water that is emanating from the gel itself, due to its swelling/shrinking. In a tight confinement, which is the situation in our experiments, this creates strong local flows whose associated viscous stresses result in a net propulsive force acting on the gel, and hence to locomotion. To verify this hypothesis, we derive a theoretical model for these flows, which we show is able to reproduce quantitatively the translational motion of the gels. Note that existing models have been developed to explain the motion of passive, strongly confined microgels in external flows.[53–55] In our case, the microgel self-propels in a quiescent fluid, and our model focuses instead on the propulsion mechanism.

We assume that the gel is quasi-2D, and that it remains symmetric with respect to the x axis, a justified approach given the centerline shapes in Fig. 1(d). In the center-of-mass body frame, a material point $\mathbf{x}$ on the surface of the gel, S, is assumed to move (due to shape changes) with velocity $\mathbf{u}_S(\mathbf{x})$, while the surface of the gel is ejecting fluid with local velocity $\phi(x)\hat{\mathbf{n}}$, where $\hat{\mathbf{n}}$ is the unit normal to S at $\mathbf{x}$, pointing into the fluid. The aim of the model is to predict the translational velocity $U(t)\mathbf{e}_x$ of the gel's center-of-mass.

To proceed, we use the theoretical framework developed for jet propulsion in the absence of inertia.[56] Following that work, we can compute the swimming speed of the gel by applying the Lorentz reciprocal theorem of Stokes flows using two flows: (i) the flow resulting from the deformation of the gel (i.e., the current problem of interest) and (ii) a second 'test' flow resulting from the translation of the gel with an arbitrary prescribed velocity $\tilde{U}\mathbf{e}_x$. Using $\tilde{\boldsymbol{\sigma}}$ to denote the stress exerted on the gel in the test flow leads to the integral identity,[56]

$$\mathbf{0} = \int_S [U\mathbf{e}_x + \mathbf{u}_S + \phi(\mathbf{x})\hat{\mathbf{n}}] \cdot \tilde{\boldsymbol{\sigma}} \cdot \hat{\mathbf{n}}\, dS. \tag{1}$$

We assume that the fluid ejection speed is uniform along the permeable sides of the microgel, and given that the flow is due to volume change in the gel, we may relate the rate of flow in and out of the gel to the rate of change of the gel length as

$$\phi = -\alpha \dot{L}, \tag{2}$$

where α is a dimensionless order-one parameter.

The relationship in Eq. (2) assumes implicitly that the rate of change of microgel's length L is the only input in the model on the fluid transport and is, therefore, sufficient to capture the asymmetry between the swelling and the shrinking process, experimentally demonstrated, for example, as the hysteresis in Fig. 1(c). In an idealized

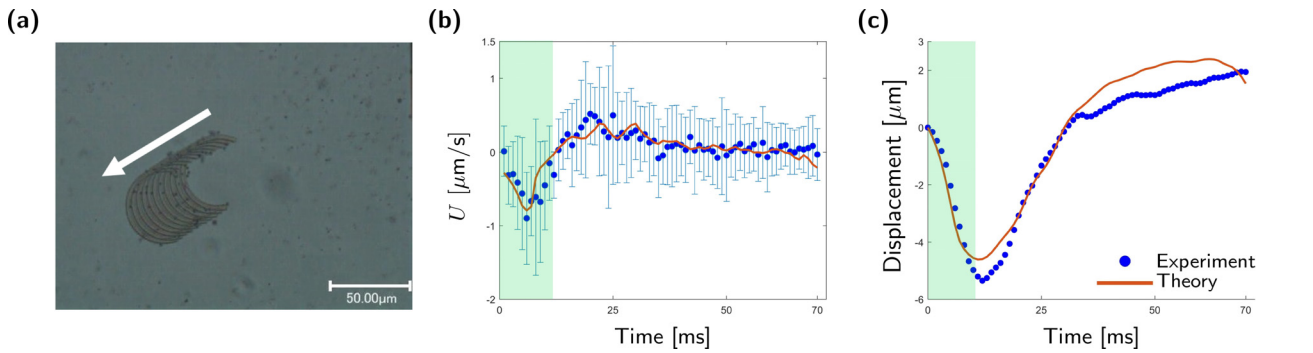

FIG. 2. Experimental (symbols) and theoretical (lines) results for the translation of the microgel for irradiation times $t_{off} = 60$ ms and $t_{on} = 10$ ms. Light green background indicates a part of the period when the laser is on. (a) Overlay of the gel shapes, sampled at the same phase of the periodic motion, with consecutive images being four periods apart. The arrow indicates the direction of motion. (b) Blue circles represent experimental results for the translational velocity; error bars represent one standard deviation in estimating the mean velocities. The solid red line represents the prediction from the theoretical model, Eq. (5) with $\alpha = 1.01$. (c) Displacement of the geometric center-of-mass of the gel during a single period, as obtained by integrating the translational velocity in time.

case, α would represent the ratio between the full cross-sectional area of the microgel and the portion of area that is permeable. However, as the geometry in our experiments is rather intricate, we let α be the only fitting parameter of the model.

The result in Eq. (1), which is a surface integral, can be next coarse-grained over the thin cross section of the gel and turned into a line integral along the length L of the gel cross section. To approximate the average of the stress $\tilde{\boldsymbol{\sigma}} \cdot \hat{\mathbf{n}}$ due to the test flow acting on a cross section, we use the resistive-force theory of slender filaments,[52] stating that $\tilde{\boldsymbol{\sigma}} \cdot \hat{\mathbf{n}} \propto (\mathbf{tt} + \Gamma \mathbf{nn}) \cdot \tilde{U}\mathbf{e}_x$. With the choice $\Gamma = 2$ (wall and unsteady effects were found to be subdominant in our comparison with the experiments), we then obtain the following integral equation:

$$0 = \int_L \left[U\mathbf{e}_x + \mathbf{u}_S - \alpha \dot{L}\mathbf{n}\right] \cdot [\mathbf{tt} + 2\mathbf{nn}] \cdot \mathbf{e}_x \, dl, \tag{3}$$

where $\mathbf{n}$ is now the unit normal pointing into the fluid but on the non-plated side of the gel, where most fluid ejection occurs, and $\mathbf{t}$ is the unit tangent along the centerline [see Fig. 1(d)]. The integral is performed along the centerline of the gel with dl being its line element. We can now use Eq. (3) to derive the instantaneous translational velocity as

$$U = \frac{2\alpha \dot{L} \int_L n_x \, dl - \int_L \mathbf{u}_S \cdot [\mathbf{tt} + 2\mathbf{nn}] \cdot \mathbf{e}_x \, dl}{\int_L (t_x^2 + 2n_x^2) \, dl}. \tag{4}$$

We note that our model does implicitly include the strong hydrodynamic confinement of the gel. The normal stresses and, therefore, the perpendicular drag force acting on a cross section are dominated by the pressure drop required to force the fluid through the narrow gap. This suggests that the integral of $\phi \hat{\mathbf{n}} \cdot \tilde{\boldsymbol{\sigma}} \cdot \hat{\mathbf{n}}$ is coarse-grained to a line integral with the integrand proportional to $\mathbf{n} \cdot \mathbf{e}_x$, as done above. The confined geometrical setup is, therefore, implicitly included in our model.

To test our theoretical prediction, we use the kinematics for the gel's centerline extracted from experimental videos. This was done using the finite difference method on the centerline shapes. The videos were recorded at the frame rate $\Delta t = 1$ ms with actuation periods $T = N\Delta t$ that were always an integer multiple of Δt. This allowed us to track the gel over many periods, so that, within each period, we record the shape at exactly the same set of phases $t_n = n\Delta t$, with $n = 0, 1, \ldots, N$. Thus, by averaging the extracted shapes and gel displacements over many periods of actuation (≈ 100), we greatly improve the accuracy of our finite difference approach.

The theoretical prediction for $U_n = U(n\Delta t)$ in Eq. (4) can then be written as

$$U_n = \alpha F_n + U_n^S, \tag{5}$$

where

$$F_n = \frac{2\dot{L} \int_L n_x \, dl}{\int_L (t_x^2 + 2n_x^2) \, dl}, \quad U_n^S = -\frac{\int_L \mathbf{u}_S \cdot [\mathbf{tt} + 2\mathbf{nn}] \cdot \mathbf{e}_x \, dl}{\int_L (t_x^2 + 2n_x^2) \, dl}, \tag{6}$$

with F_n representing the contribution due to the fluid transport through the surface of the gel and U_n^S that due to the evolution of the shape. Note that taking $F_n = 0$ is equivalent to assuming the locomotion is due solely to the non-reciprocal shape changes, which is not able to reproduce our experimental results (see above).

The only free parameter in the model is the order-one dimensionless constant of proportionality α from Eq. (2). We fix its value by performing a least-square fitting on the model given by Eq. (5), where U_n is extracted from the experiments, while F_n and U_n^S are computed using the kinematics extracted from the experimental data, as described above. The optimal value of α was found to be slightly different for different experimental conditions, which is not surprising, given that it encapsulates complicated and highly sensitive microgel swelling/shrinking dynamics.

In Figs. 2(b) and 2(c), we show the comparison between the experimental data (blue symbols) and the theoretical model (solid red line). Our theoretical prediction for the translational velocity is in excellent agreement with the experimental results for both the instantaneous value of the velocity [Fig. 2(b)] and the total integrated displacements [Fig. 2(c)]. Moreover, we obtain the same level of agreement in an experiment with a different set of irradiation times that lead to a significant rotation of the microgel (see Fig. S1 in the supplementary material).

We further investigate the hydrodynamics of swimming by predicting theoretically the fluid flow around a cross section of the microgel. As a model system, we assume that the cross section of the gel is circular ('disk' in what follows) of radius r_0 and is ejecting (taking in) fluid at speed U_0 from the part of its perimeter that describes an angle $2\beta < 2\pi$ [see sketch in Fig. 3(a)]. As the fluid is ejected (taken in), the radius of the gel must change as $\dot{r}_0 = -\beta U_0/\pi$ due to the conservation of volume. In an unbounded fluid, an analytic solution exists for the flow around this two-dimensional setup.[57] Under the assumption of zero net hydrodynamic force, the disk translates with velocity $-U_0 \sin\beta/\pi$ and drives a two dimensional flow $u\hat{\mathbf{r}} + v\hat{\boldsymbol{\theta}}$ in polar coordinates given by

$$\frac{u}{U_0} = \frac{\sin\beta\cos\theta}{\pi}\left(\frac{r_0}{r}\right)^2 + \sum_{n=2}^{\infty} \frac{\sin n\beta \cos n\theta}{\pi n}\left[n\left(\frac{r_0}{r}\right)^{n-1} - (n-2)\left(\frac{r_0}{r}\right)^{n+1}\right], \tag{7}$$

$$\frac{v}{U_0} = \frac{\sin\beta\sin\theta}{\pi}\left(\frac{r_0}{r}\right)^2 + \sum_{n=2}^{\infty} \frac{n-2}{\pi n} \sin n\beta \sin n\theta \left[\left(\frac{r_0}{r}\right)^{n-1} - \left(\frac{r_0}{r}\right)^{n+1}\right]. \tag{8}$$

We illustrate this unbounded flow (non-dimensionalized by U_0) in Fig. 3(b) in the case $\beta = 2\pi/3$ (the flow shown is the series truncated at order $(r_0/r)^n$, with $n = 40$).

If we now confine the disk between rigid surfaces, the strongest flow occurs in the narrow gaps between the disk and the walls, and the analytical solution that could capture this part of the flow would be cumbersome. To gain intuition about flow features in this case, we use COMSOL[58] to solve for the Stokes flow under the same situation (i.e., force-free locomotion of the disk with $\beta = 2\pi/3$) for a disk symmetrically located in a space of size $2r_0/0.9$ between two rigid surfaces. We show in Fig. 3(c) the streamlines and the magnitude of the flow, illustrating the strong flows that are locally induced in the tight space

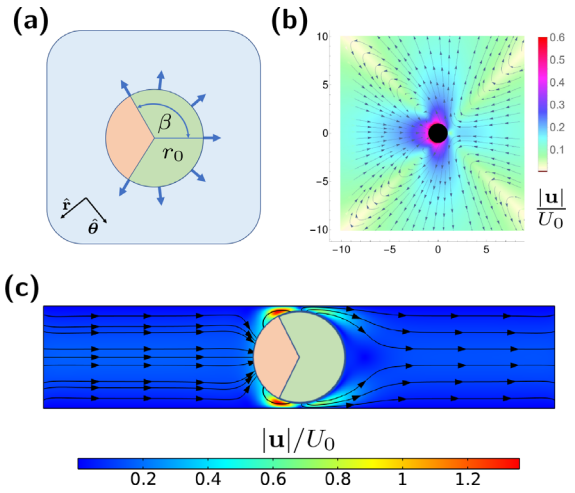

FIG. 3. Using a two-dimensional model where the gel expels flow uniformly along its surface (a), we show the flow induced around the circular cross section in an unbounded fluid [(b), analytical solution] and in the tight space between two rigid surfaces [(c), numerical computations]. (a) Sketch of a toy model of a cross section with surface angle $2\beta < 2\pi$ expelling fluid. (b) Flow around the model cross section in an unbounded domain, given by Eqs. (7) and (8) for $\beta = 2\pi/3$. Arrows represent the flow direction, while colors indicate the flow magnitude non-dimensionalized by U_0. (c) Results of COMSOL[58] simulations for a model cross section ($\beta = 2\pi/3$) in the presence of two no-slip plane walls (top and bottom). Lines show streamlines, while colors indicate the flow magnitude non-dimensionalized by U_0 (spacing between the walls of $2r_0/0.9$).

between the disk and the surfaces and their right-left asymmetry—this is the physical origin of the net propulsion.

In summary, in this paper, we report a jet-driven type of microgel propulsion. In contrast with many studies of artificial swimming, which rely on the non-reciprocal bending of the centerline of slender swimmers to swim, here locomotion is driven by the localized fluid transport in and out of the gel caused by its rapid swelling and deswelling. This viscous-jet hypothesis is confirmed to be the dominant mechanism of propulsion by a hydrodynamic model that shows excellent agreement with our experimental results.

See the supplementary material for details of the experimental methods.

This project has received funding from the European Research Council under the European Union's Horizon 2020 Research and Innovation Programme (Grant No. 682754 to E.L.) and from Trinity College, Cambridge (IGS scholarship to I.T.). This research was supported by the German Science Foundation, through the priority program on microswimmers under Grant No. 255087333. We have also benefited from the thriving scientific environment provided by the SFB 985 on functional microgels and microgel systems.

AUTHOR DECLARATIONS

Conflict of Interest

The authors have no conflict of interest to declare.

DATA AVAILABILITY

The data that support the findings of this study are available from the corresponding author upon reasonable request.

REFERENCES

[1]D. Bray, *Cell Movements* (Garland Publishing, New York, 2000).
[2]J. S. Guasto, R. Rusconi, and R. Stocker, "Fluid mechanics of planktonic microorganisms," Annu. Rev. Fluid Mech. **44**, 373–400 (2012).
[3]G. Taylor, "Analysis of the swimming of microscopic organisms," Proc. R. Soc. London Ser. A **209**, 447–461 (1951).
[4]J. Gray and G. J. Hancock, "The propulsion of Sea-urchin spermatozoa," J. Exp. Biol. **32**, 802–814 (1955).
[5]J. Lighthill, *Mathematical Biofluiddynamics* (SIAM, Philadelphia, 1975).
[6]E. Lauga, *The Fluid Dynamics of Cell Motility* (Cambridge University Press, UK, 2020).
[7]T. J. Pedley and J. O. Kessler, "Hydrodynamic phenomena in suspensions of swimming microorganisms," Annu. Rev. Fluid Mech. **24**, 313–358 (1992).
[8]R. E. Goldstein, "Green algae as model organisms for biological fluid dynamics," Annu. Rev. Fluid Mech. **47**, 343–375 (2015).
[9]E. Lauga, "Bacterial hydrodynamics," Annu. Rev. Fluid Mech. **48**, 105–130 (2016).
[10]E. Gaffney, H. Gadêlha, D. Smith, J. Blake, and J. Kirkman-Brown, "Mammalian sperm motility: Observation and theory," Annu. Rev. Fluid Mech. **43**, 501–528 (2011).
[11]L. J. Fauci and R. Dillon, "Biofluidmechanics of reproduction," Annu. Rev. Fluid Mech. **38**, 371–394 (2006).
[12]K. M. Ottemann and J. F. Miller, "Roles for motility in bacterial–host interactions," Mol. Microbiol. **24**, 1109–1117 (1997).
[13]M. Kim, A. Julius, and U. Cheang, *Microbiorobotics: Biologically Inspired Microscale Robotic Systems, Micro and Nano Technologies* (Elsevier Science, 2017).
[14]W. Hu, G. Lum, M. Mastrangeli, and M. Sitti, "Small-scale soft-bodied robot with multimodal locomotion," Nature **554**, 81–85 (2018).
[15]R. Dreyfus, J. Baudry, M. Roper, M. Fermigier, H. Stone, and J. Bibette, "Microscopic artificial swimmers," Nature **437**, 862–865 (2005).
[16]B. Williams, S. Anand, J. Rajagopalan, and M. Saif, "A self-propelled biohybrid swimmer at low reynolds number," Nat. Commun. **5**, 3081 (2014).
[17]H.-W. Huang, M. Sakar, A. Petruska, S. Pané, and B. Nelson, "Soft micromachines with programmable motility and morphology," Nat. Commun. **7**, 12263 (2016).
[18]M. Sitti, H. Ceylan, W. Hu, J. Giltinan, M. Turan, S. Yim, and E. Diller, "Biomedical applications of untethered mobile milli/microrobots," Proc. IEEE **103**, 205–224 (2015).
[19]J. Li, B.-F. Ávila, W. Gao, L. Zhang, and J. Wang, "Micro/nanorobots for biomedicine: Delivery, surgery, sensing, and detoxification," Sci. Rob. **2**, eaam6431 (2017).
[20]B. Nelson, I. Kaliakatsos, and J. Abbott, "Microrobots for minimally invasive medicine," Annu. Rev. Biomed. Eng. **12**, 55–85 (2010).
[21]E. M. Purcell, "Life at low reynolds number," Am. J. Phys. **45**, 3–11 (1977).
[22]E. Lauga, "Life around the scallop theorem," Soft Matter **7**, 3060–3065 (2011).
[23]L. Becker, S. Koehler, and H. Stone, "On self-propulsion of micro-machines at low Reynolds number: Purcell's three-link swimmer," J. Fluid Mech. **490**, 15–35 (2003).
[24]D. Tam and A. Hosoi, "Optimal stroke patterns for Purcell's three-link swimmer," Phys. Rev. Lett. **98**, 068105 (2007).
[25]J. Avron and O. Raz, "A geometric theory of swimming: Purcell's swimmer and its symmetrized cousin," New J. Phys. **10**, 063016 (2008).
[26]A. Najafi and R. Golestanian, "Simple swimmer at low Reynolds number: Three linked spheres," Phys. Rev. E **69**, 062901 (2004).
[27]R. Dreyfus, J. Baudry, and H. Stone, "Purcell's 'rotator': Mechanical rotation at low Reynolds number," Eur. Phys. J. B **47**, 161–164 (2005).
[28]R. Golestanian, "Synthetic mechanochemical molecular swimmer," Phys. Rev. Lett. **105**, 018103 (2010).
[29]J. Avron, O. Kenneth, and D. Oaknin, "Pushmepullyou: An efficient micro-swimmer," New J. Phys. **7**, 234 (2005).

[30]A. Najafi and R. Zargar, "Two-sphere low-Reynolds-number propeller," Phys. Rev. E **81**, 067301 (2010).
[31]M. Iima and A. Mikhailov, "Propulsion hydrodynamics of a butterfly micro-swimmer," Europhys. Lett. **85**, 44001 (2009).
[32]C. Wiggins and R. Goldstein, "Flexive and propulsive dynamics of elastica at low Reynolds number," Phys. Rev. Lett. **80**, 3879–3882 (1998).
[33]M. Manghi, X. Schlagberger, and R. Netz, "Propulsion with a rotating elastic nanorod," Phys. Rev. Lett. **96**, 068101 (2006).
[34]B. Qian, T. Powers, and K. Breuer, "Shape transition and propulsive force of an elastic rod rotating in a viscous fluid," Phys. Rev. Lett. **100**, 078101 (2008).
[35]A. Cebers, "Flexible magnetic filaments," Curr. Opin. Colloid Interface Sci. **10**, 167–175 (2005).
[36]S. Childress and R. Dudley, "Transition from ciliary to flapping mode in a swimming mollusc: Flapping flight as a bifurcation in re_ω," J. Fluid Mech. **498**, 257–288 (2004).
[37]E. Lauga, "Continuous breakdown of purcell's scallop theorem with inertia," Phys. Fluids **19**, 061703 (2007).
[38]E. Lauga, "Life at high Deborah number," Europhys. Lett. **86**, 64001 (2009).
[39]E. Lauga, "Locomotion in complex fluids: Integral theorems," Phys. Fluids **26**, 081902 (2014).
[40]S. V. Nikolov, P. D. Yeh, and A. Alexeev, "Self-propelled microswimmer actuated by stimuli-sensitive bilayered hydrogel," ACS Macro Lett. **4**, 84–88 (2015).
[41]A. Mourran, H. Zhang, R. Vinokur, and M. Möller, "Soft microrobots employing nonequilibrium actuation via plasmonic heating," Adv. Mater. **29**, 1604825 (2017).
[42]H. Zhang, A. Mourran, and M. Möller, "Dynamic switching of helical microgel ribbons," Nano Lett. **17**, 2010–2014 (2017).
[43]L. Koens, H. Zhang, M. Moeller, A. Mourran, and E. Lauga, "The swimming of a deforming helix," Eur. Phys. J. E **41**, 119 (2018).
[44]A. Mourran, O. Jung, R. Vinokur, and M. Möller, "Microgel that swims to the beat of light," Eur. Phys. J. E **44**, 79 (2021).
[45]P. J. Flory and J. Rehner, "Statistical mechanics of cross–linked polymer networks II. Swelling," J. Chem. Phys. **11**, 521–526 (1943).
[46]Y. Li and T. Tanaka, "Phase transitions of gels," Annu. Rev. Mater. Sci. **22**, 243–277 (1992).
[47]M. Doi, "Gel dynamics," J. Phys. Soc. Jpn. **78**, 052001 (2009).
[48]C.-Y. Hui and V. Muralidharan, "Gel mechanics: A comparison of the theories of biot and Tanaka, Hocker, and Benedek," J. Chem. Phys. **123**, 154905 (2005).
[49]J. P. Rolland, B. W. Maynor, L. E. Euliss, A. E. Exner, G. M. Denison, and J. M. DeSimone, "Direct fabrication and harvesting of monodisperse, shape-specific nanobiomaterials," J. Am. Chem. Soc. **127**, 10096–10100 (2005).
[50]H. Zhang, L. Koens, E. Lauga, A. Mourran, and M. Moeller, "A light-driven microgel rotor," Small **15**, 1903379 (2019).
[51]X.-Z. Zhang, X.-D. Xu, S.-X. Cheng, and R.-X. Zhuo, "Strategies to improve the response rate of thermosensitive pnipaam hydrogels," Soft Matter **4**, 385–391 (2008).
[52]R. G. Cox, "The motion of long slender bodies in a viscous fluid Part 1. General theory," J. Fluid Mech. **44**, 791–810 (1970).
[53]M. Nagel, P.-T. Brun, H. Berthet, A. Lindner, F. Gallaire, and C. Duprat, "Oscillations of confined fibres transported in microchannels," J. Fluid Mech. **835**, 444–470 (2018).
[54]M. Bechert, J. Cappello, M. Daïeff, F. Gallaire, A. Lindner, and C. Duprat, "Controlling transport dynamics of confined asymmetric fibers," Europhys. Lett. **126**, 44001 (2019).
[55]J. Cappello, M. Bechert, C. Duprat, O. du Roure, Fmc. Gallaire, and A. Lindner, "Transport of flexible fibers in confined microchannels," Phys. Rev. Fluids **4**, 034202 (2019).
[56]S. E. Spagnolie and E. Lauga, "Jet propulsion without inertia," Phys. Fluids **22**, 081902 (2010).
[57]J. Blake, "Self propulsion due to oscillations on the surface of a cylinder at low Reynolds number," Bull. Australian Math. Soc. **5**, 255–264 (1971).
[58]COMSOL Multiphysics® v. 5.6 (COMSOL AB, Stockholm, 2020), available at https://www.comsol.com/.